Design of a series elastic actuator for a compliant parallel wrist rehabilitation robot

Fabrizio Sergi, Melissa M. Lee, and Marcia K. O'Malley

Abstract— **This paper presents the design of a novel linear series elastic actuator purposely designed to match the requirements of robots for wrist rehabilitation: backdriveability, intrinsic compliance, and capability to be controlled as ideal force/torque sources. An existing rehabilitation robot is adapted to include intrinsic compliance in the design. A novel linear compliant element is designed to meet dimensional and force/stiffness requirements; a force sensing scheme involving a Hall-effect sensor is optimized in FEM simulations and developed. Linearity tests of the compliant sensing element show a maximum of 4.5% of FSO combined nonlinearity and hysteresis errors. Characterization experiments show that the developed system introduces physical compliance, still guaranteeing accurate force control in a frequency range largely compatible with that required for wrist assistance during rehabilitation.**

I. INTRODUCTION

Rehabilitation robotics is essentially centered around one robot behavior: human-robot physical interaction. Hence, it appears straightforward to deploy interaction control schemes in rehabilitation robots [1]. In the rehabilitation scenario, such control schemes assist motion by applying variable levels of mechanical assistance, with the capability of adapting to and capitalizing on the residual contributions of the subjects. Moreover, evidence from human trials with stroke subjects [2] and from preliminary studies on animal models of spinal cord injury (SCI) [3] confirms the hypothesis that interaction control schemes are more capable of promoting plasticity through mechanical interaction compared to motion control.

Interaction control laws such as impedance control [4] can be implemented easily and accurately in the case of manipulators with negligible intrinsic dynamical properties. If the latter condition is not met, however, model-based dynamic compensation schemes for impedance control need to be adopted [5]. Such approaches bring the consequence of accuracy loss due to modeling inaccuracies, or neglect of higher order or nonlinear dynamical effects. To overcome the mentioned limitations, force-feedback control schemes can be used to improve the accuracy of interaction control in non transparent manipulators. In force-feedback control, the force of interaction between the robot and the environment is measured and fed back to the controller driving the actuators, which specifies new desired force or position/velocity commands.

The proper design of rehabilitation robots needs to consider the biomechanical properties of the addressed segments and joints in the definition of design specifications. In the case of the wrist joint, several biomechanical studies have highlighted how wrist intrinsic dynamical properties are dominated by stiffness [6], [7], [8]. The value of physical stiffness measured for the resting wrist joint for flexion/extension and radial/ulnar deviation is comprised in the range [0.5-2] N·m/rad, and is a function of the wrist pose and of neighboring joints poses, such as the index finger joint. Thus, it seems likely that the application of support schemes based on physical compliance can help restore neuromechanical capabilities in a more efficient and bio-inspired way.

The Series Elastic Actuation (SEA) architecture [9], [10] allows fulfillment of all the above-mentioned requirements for rehabilitation robots. In SEAs, compliant elements with deflection/force measurement capabilities are intentionally introduced in series between the actuator and the load, effectively acting as a mechanical filter that decouples the non-linearities of geared actuators from the output and enables implementation of force-feedback control laws. The introduction of physical compliance with well known properties enables the deployment of accurate interaction control schemes, thus mimicking the traditional therapist-based physical therapy, essentially based on the adaptive and compliant transfer of support forces.

The goal of this project is to develop a *force-feedback, series-elastic* version of a currently existing device, the RiceWrist [11], a parallel wrist exoskeleton previously developed at Rice University and currently clinically used for wrist rehabilitation after SCI and stroke.
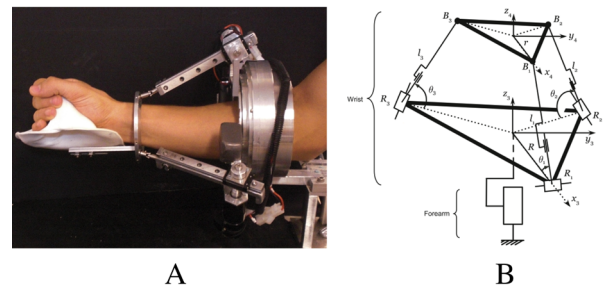

Fig. 1. (A) Prototype of the RiceWrist and (B) schematic of the serial-in-parallel manipulator. For the parallel structure, variables l_1, l_2 and l_3 are actuated, while the moving platform orientation is defined by α and β angles of a Euler sequence $R_\alpha(x)R_\beta(y)R_\gamma(z)$; these are the end-effector coordinates.

II. DESIGN

A. Definition of design specifications

The design pursued in this work is based on the RiceWrist [11], which is a serial-in-parallel, four degree-of-freedom (DOF) robotic manipulator, designed to provide support to wrist movements during rehabilitation. When worn by a subject, its DOFs decrease to three (translation along the radial axis is ideally prevented by the anatomy of the wrist joint) and supports wrist movements in a range of motion compatible with that of the wrist joint during basic activities. The kinematic structure of the RiceWrist is well suited for the introduction of elasticity in series to the linear actuators, and it has been unaltered in the compliant version.

In series elastic robots for human interaction, physical compliance should be ideally introduced as close as possible to the user, i.e., at the far end of the actuation architecture, thus allowing implementation of force-feedback control schemes based on a direct and accurate measurement of interaction force. In the described actuation system, this design target could be achieved by including a compliant force-sensing element in series between the moving platform and the handle. As an example, an off-the-shelf 6-axis force sensor would allow to match this requirement; in this case, however, the intrinsic stiffness introduced would be much higher than desired, allowing not to realize a proper series-elastic actuation architecture, but only a force-feedback controlled device.

In the present work, a simpler solution was adopted, which consists of the inclusion of bidirectional linear springs in series with the three linear actuators of the parallel portion of the manipulator. In this scheme, a transmission stage is included between the physical compliance and the load, namely the three spherical joints. However, such joints have negligible friction and non-linearities, thus guaranteeing a high level of accuracy of force-feedback controllers based on actuator force measurement. The adoption of such a sensing scheme allows improvement of force transfer fidelity over the current version, and achievement of the desired intrinsic compliance. It has to be noted that the pursued topology does not allow any physical series elasticity for forearm pronation/supination. However, that specific movement is actually supported by a direct-drive actuator, implying that accurate force transfer capability can be achieved when implementing virtual stiffness control on this degree of freedom. The pursued approach allows for achievement of at least a subset of the design requirements (e.g., accurate force control).

Having defined the mechanism topology, we now define quantitative requirements for the compliant sensing elements.

1) Force-torque range: Biomechanical analyses of Activities of Daily Living (ADL) show that torque transfer requirements for the wrist joints are modest, with a maximum of 0.35 N·m required for flexion/extension and radial/ulnar deviation and only 0.06 N·m required for forearm pronation/supination [12]. However, torques applied during rehabilitation therapy with impaired subjects are in the order
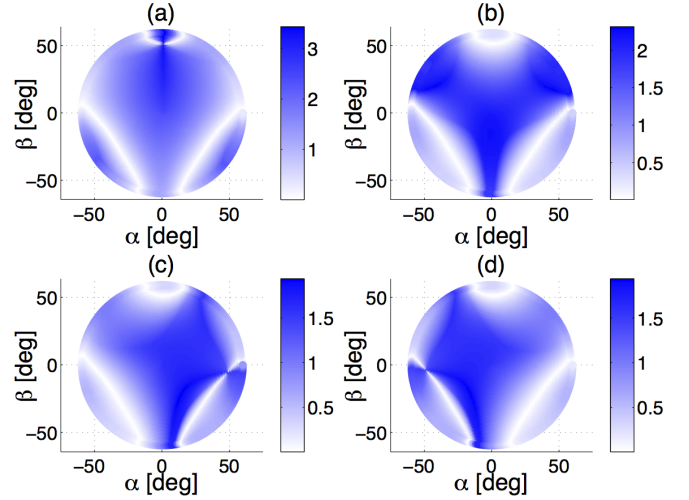

Fig. 2. Maximum transferrable torque due to actuators force saturation (set to 20 N) for different values of flexion/extension (α) and radio-ulnar deviation (β), for different desired torque conditions. The blue colormap represents the peak continuous torque, in N·m, for the following conditions: (a) maximum flexion/extension torque; (b) maximum radial/ulnar deviation torque; transfer of an equal torque along the flexion/extension and radial/ulnar deviation axes with the same (c) or opposite (d) sign. White regions represent singularities of the manipulator, that are excluded from the reachable workspace by mechanical end-stops.

of 1-1.5 N·m, comparable with that reported by other wrist rehabilitation devices [13]. Since a parallel structure has been selected for the Series Elastic RiceWrist, it is not possible to describe the force/torque saturation capabilities in output coordinates in a simple manner as it is for serial robots (one scalar for every actuated DOF), since the maximum transferrable force is a function of the independent generalized coordinates $\mathbf{q}$, which may include actuated (input) coordinates (the vector $\mathbf{l} = [l_1, l_2, l_3]^T$ in our case) or end-effector coordinates $\mathbf{x} = [\alpha, \beta, Z_c]^T$. In static conditions, having defined the vector $\mathbf{F_l} = [f_1, f_2, f_3]^T$ of forces applied by the actuators, the reflected force/torque in output coordinates is $\mathbf{T_x} = [T_\alpha, T_\beta, F_z]^T$, where $\mathbf{F_l} = \mathbf{J(q)^T T_x}$, and $\mathbf{J(q)} = \frac{\partial \mathbf{x}}{\partial \mathbf{l}}$. Figure 2 shows the effect of actuator force saturation on transferred torque for representative cases involving only flexion/extension, radio/ulnar deviation, and two combinations of the former. It is possible to see that the desired torque transfer capabilities can be obtained by limiting actuator force to 20 N, which will be set as a design requirement.

2) Stiffness range: SEA physical stiffness needs to be carefully selected to trade off intrinsic compliance, accuracy of force measurement, displacement range and bandwidth of force control [9], [10], [14], [15]. Furthermore, when addressing rehabilitation of joints with intrinsic compliance, the values of physical stiffness of the human counterpart in resting and pathological conditions also needs to be taken into account. In this research, the physical stiffness design target value was specified in order to obtain approximately twenty times the physical stiffness of the resting human wrist,
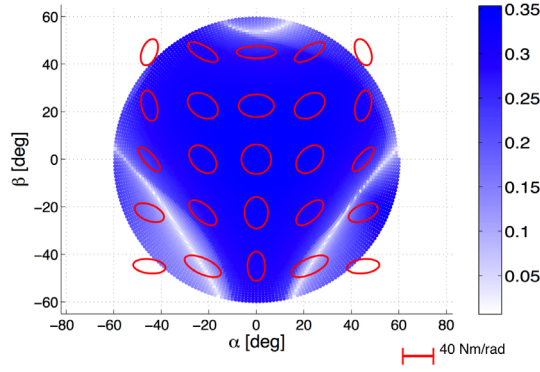
Fig. 3. Stiffness ellipses in end-effector coordinates, deriving from actuator stiffnesses $k_1 = k_2 = k_3 = 5.5 \cdot 10^3$ N/m, overlaid over a metric of robot manipulability, the condition number [19], defined as $\kappa = \sqrt{(\lambda_{min}/\lambda_{max})}$, with λ being the eigenvalues of the $\mathbf{J}^{-\mathbf{T}}\mathbf{J}^{-1}$ matrix. The scale bar reports the scaling of stiffness ellipses eigenvalues. Acceptable values of manipulability are obtained in a circle in end-effector rotation coordinates with radius of 45 degrees, that defines the usable workspace of the robot.

Fig. 4. Force vs. length plot of the springs selected, and of their parallel connection.

so as to guarantee a wide range of virtual stiffness to be implemented with linear, passivity-based controllers such as the one proposed by [16], [17]. However, this requirement does not directly translate into values of physical stiffness for the linear compliant elements, due to the non-linear mapping between stiffness in input and output coordinates introduced by the parallel manipulator. By defining $\mathbf{K_l} = \mathrm{diag}(k_1, k_2, k_3)$ the vector of physical stiffness included in series with the three actuators, the reflected stiffness matrix in output coordinates can be calculated as $\mathbf{K_x} = (\mathbf{J(q)}^{-1})^{\mathbf{T}}\mathbf{K_l}\mathbf{J}^{-1}(\mathbf{q})$ [18]. This implies that the constant stiffness in actuator coordinates is mapped non-uniformly in end-effector coordinates, as shown in Figure 3. In order to determine approximate design requirements, a target value of equivalent physical stiffness of 40 N·m/rad was specified for both flexion/extension and radial/ulnar deviation (in the center of the workspace), with corresponding values of linear stiffnesses in actuator coordinates of $5.2 \cdot 10^3$ N/m.

3) Maximum resting length: With the reported linear stiffness requirement, the maximum deflection of the compliant element at the maximum loading condition (20 N) is approximately equal to 3.6 mm. However, the total length added by the introduction of the elastic element in series is longer due to the space needed for supporting elements and also due to the physical resting length of deflecting elements. Typical compliant elements for linear SEAs are obtained by interposing in series two commercial compression springs. However, this scheme implies a noticeable increase of the overall maximum length, which can be up to several times the desired deflection. In the case of the RiceWrist, an increase in the minimum length of actuated joints R_iB_i can lead to a reduction of the available workspace, since the minimum length of vectors B_iR_i during operation is equal to 80 mm. Considering that the chosen cable-and-slider transmission introduces a "dead-length" of approximately 30
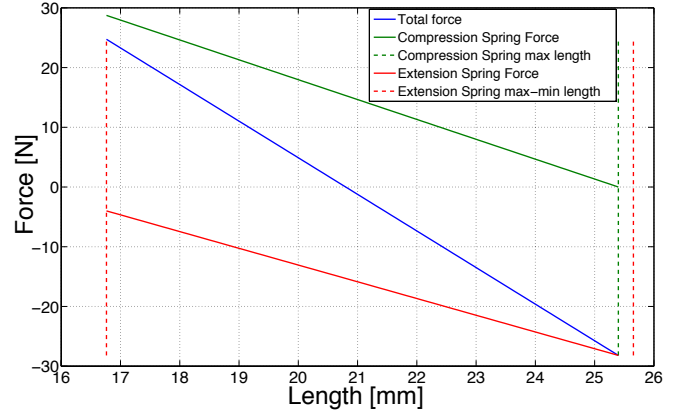
mm, this leaves a maximum admissible length of less than 50 mm for the compliant element, that will be reduced to 30 mm as design requirement, so as to allow margin for inclusion of subjects with different anthropometric sizes.

B. Implementation

The above-described design requirements were matched by a solution comprising the parallel connection of two commercial springs, a compression spring and an extension spring. This configuration allows minimization of resting length, as desired for workspace maximization, without increasing the lateral dimension, since the two springs can be mounted concentrically on the same support. This simple and cost effective configuration increases the elastic energy stored per unit volume, without requiring the design of custom components. Moreover, the inclusion of pre-loaded elastic elements guarantees a zero dead band non-linearity introduced by backlash in the shaft-spring connection, without requiring high manufacturing tolerances. Two commercial springs (Century Spring Corp.) were selected in order to match both maximum force and stiffness requirements, resulting in the mechanical properties defined in Table I.

The parallel connection of these two springs results in a bidirectional linear compliant element with a force range higher than ±20 N and a 6.5 mm deflection range, with a resulting stiffness of 6 N/mm. These characteristics are within 15% of the design specification. The theoretical force vs. displacement relationship for the compliant element is described in Figure 4.

A miniaturized support has been designed in order to allow

TABLE I

PROPERTIES OF SELECTED TENSION AND COMPRESSION SPRINGS

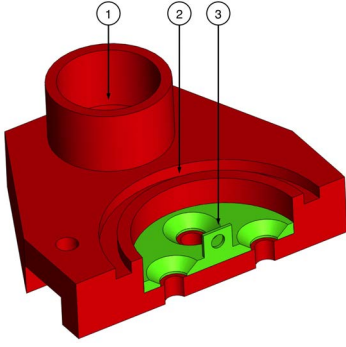|	Compression spring	Extension spring
Resting length [mm]	25.4	16.7
Stiffness [N/mm]	3.3	2.7
Maximum force [N]	53.4	29
Engagement force [N]	-	4

Fig. 5. 3D CAD section of the support for one end of the springs. (1) Support for the linear bearings, (2) groove for compression spring mounting, (3) hook for extension spring support.
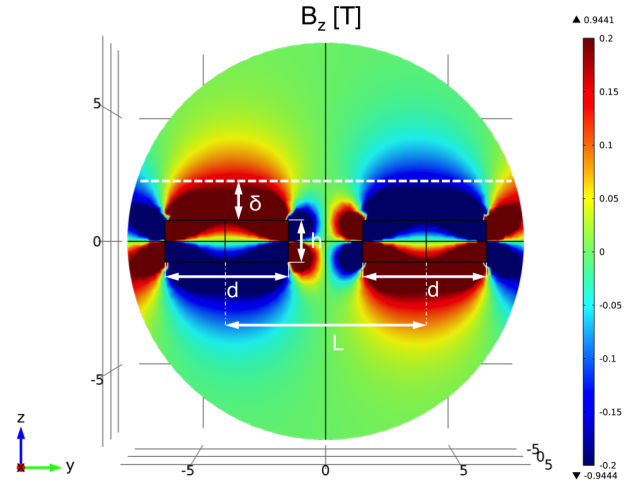

Fig. 6. Distribution of the z-component of magnetic field density vector $\mathbf{B}$. The moving Hall effect sensor measures the component along the line at a distance δ from the magnets surface.

mounting the two springs in parallel, while guaranteeing a high lateral stiffness. The support comprises two mounting plates, with circular grooves that allow mounting the compression spring by interference through its flattened edge. The extension spring is supported by a second set of support plates, concentric to the first two, that feature a hole where the extension spring hook engages. Two precision linear ball bearings (SKF LBXR 2G/HV6, 3.2 mm nominal diameter) and mating precision shafts are also included, so as to guarantee the desired lateral stiffness, effectively limiting the degree of mobility of the mechanism to purely translational motion. A 3D CAD section of one of the two supports is shown in Figure 5.

C. Force sensing

Force-feedback control using an SEA requires directly measuring spring deflection, or accurately measuring the absolute rotation of motor and load positions and inferring the deflection by difference. However, the first option is preferable when possible (as already suggested by [10]), so to avoid noise due to encoder quantization. A non-contact sensorization option is also preferable, so to avoid the inclusion of friction in parallel to the force measurement.

In this paper, a novel non-contact sensing scheme for a linear compliant force/displacement sensor has been developed, based on an optimized magnetic system. Two identical cylindrical neodymium magnets (diameter d, height h), axially magnetized, are mounted at a distance L in a nonmagnetic support so that their magnetization axes are antiparallel (see Figure 6). The profile of magnetic field density on a line at a distance δ from the base of the cylinders, along a direction parallel to the x axis, is nonlinear, but can be well approximated with a linear expression in a big-enough displacement range.

A static Magnetic field FEM analysis has been conducted using COMSOL Multiphysics (COMSOL Inc.) using a stationary solver (fgmres) and specifying the magnetization condition of the permanent magnets in the form:

$$\mathbf{B} = \mu_0\mu_r\mathbf{H} + \mathbf{B_r}, \tag{1}$$

with $\mathbf{B}$ magnetic flux density (T), $\mathbf{H}$ magnetic field (A/m^2) and $\mathbf{B_r}$ magnet remanent flux density, in Tesla. A surrounding sphere of air with $\epsilon_r = \mu_r = 1$ was specified as an additional subdomain, where the resulting flux density was calculated.

The design was optimized considering as parameters d, L and h and $\mathbf{B_r}$, in order to obtain good linearity in the required range (± 3.5 mm) and magnetic flux density values measurable using off-the-shelf Hall effect sensors (typical range: $\pm$ 100 mT). The optimized configuration includes commercial magnets from K&J Magnetics Inc. grade N52, with $d = 4.8$ mm, $h = 1.59$ mm, placed at a distance $L = 8.9$ mm, that provide the voltage vs. distance curves shown in Figure 7, parameterized as a function of the distance δ, calculated through static FEM simulations. A linear fit was applied to each of the curves (in the required range), obtaining the goodness of fit properties summarized in Table II. The three solutions with higher δ provide an acceptable nonlinearity error (less than 3% of Full Scale Output). Among them, the solution with $\delta = 2.54$ mm maximizes sensitivity while providing magnetic field signals in the range of small-size Hall-effect sensors. For this reason, this configuration was selected for the design of the real prototype, shown in Figure 8, whose overall dimensions are

TABLE II
THEORETICAL MAGNETIC FIELD DENSITY VS. POSITION PROFILES

δ [mm]	R^2	Max nonlinearity [mm]	Sensitivity [mT/mm]
3.05	0.996	0.167	18.1
2.79	0.996	0.171	21.6
2.54	0.996	0.194	25.8
2.29	0.995	0.2	31.0
2.03	0.992	0.28	37.0
1.78	0.9868	0.4	44.3
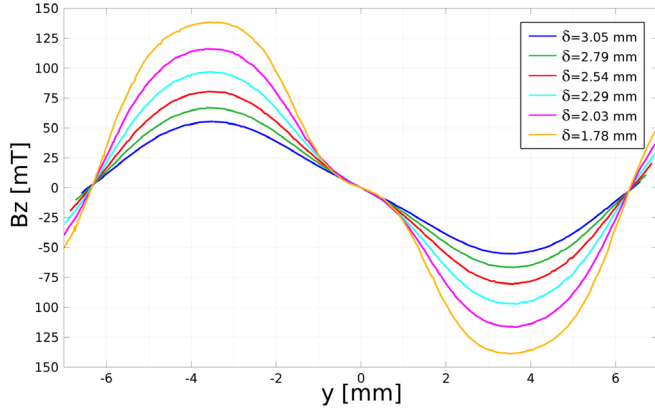
Fig. 7. $\mathbf{B_z}$ measured over a line at a distance δ from the magnets surface.

Fig. 9. Force vs. displacement curve for the compliant element, deriving from the hysteresis test comprising extension from 0 to 20 N, then compression from 20 N to -20 N, finally extension from -20 N to 0.

40mm $\times$ 24mm $\times$ 30mm.

III. DESIGN VALIDATION

A. Compliant force sensor characterization

The fabricated compliant force sensor has been validated using an Instron machine equipped with a Instron 158 load cell. The moving plate of the machine was moved continuously at a velocity of 1mm/min. An hysteresis test was conducted by moving the plate initially in the extension direction, until the recorded force exceeded 20 N, then movement was reversed to reach the maximum compression force of -20 N, and eventually the part was gradually unloaded to 0 N. Force was measured and recorded by the Instron machine continuously at 30 samples/s. The acquired data was filtered using a symmetric moving average filter in a temporal window of 1 s to remove load cell noise. Position versus force profiles were thus extracted, producing the plot in Figure 9, showing a good linearity throughout the range, with negligible effects of hysteresis and zero backlash. A linear fit gives an R^2 value of 0.999 and a maximum combined nonlinearity and hysteresis error of 0.5 N, or 2.5% of FSO.
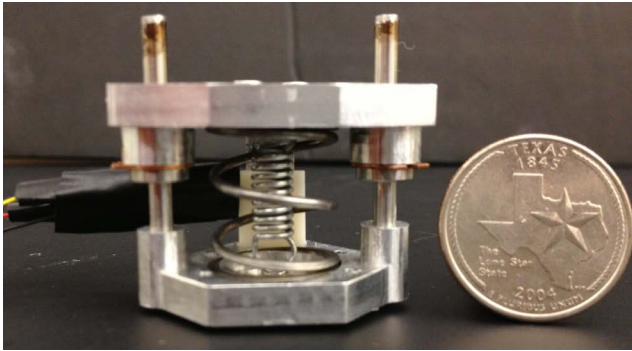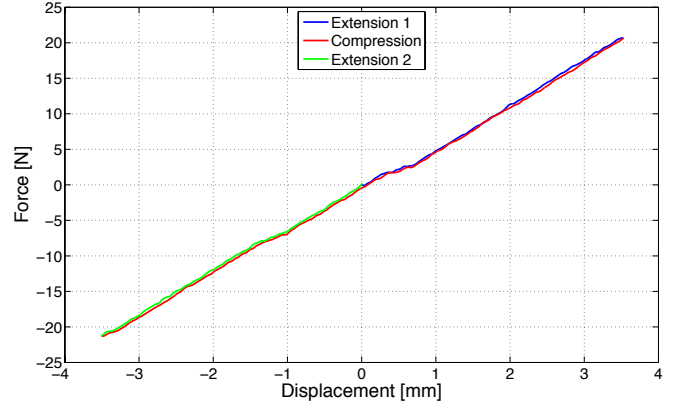

Fig. 8. Prototype of the sensorized spring for the Series Elastic RiceWrist. Dimensions are 40mm (width), 24mm (depth), 30 mm (height in fully extended configuration). Supports for the magnets (aluminum) and Hall-effect sensor (white ABS) are visible behind the springs.

The voltage measured by the Hall-effect sensor was measured continuously during the experiment; data corresponding to increments or decrements of 0.25 mm were recorded and correlated with the force measured by the load cell, providing the sensor calibration curve, shown in Figure 10. A linear fit provides an R^2 coefficient of 0.996, and a maximum of 0.9 N nonlinearity and hysteresis error, corresponding to 4.5% FSO. This linear profile will be used to infer force for the experiments reported in the following section.

B. Force bandwidth characterization

A 1 DOF test-bed was developed to evaluate the force feedback regulation performance of the designed SEA. A brushed DC motor (RE40, Maxon Motors Corp.) is supported by a rigid frame; a threaded spool is mounted on its shaft, onto which a cable converts motor rotation into the translation of a slider supported by a linear bearing. The compliant force sensor is mounted on the output of the linear slider in order to measure the force of interaction with the environment along the actuated DOF. A force-feedback control scheme is used to drive the motor, using the measurement obtained from the Hall-effect sensor and
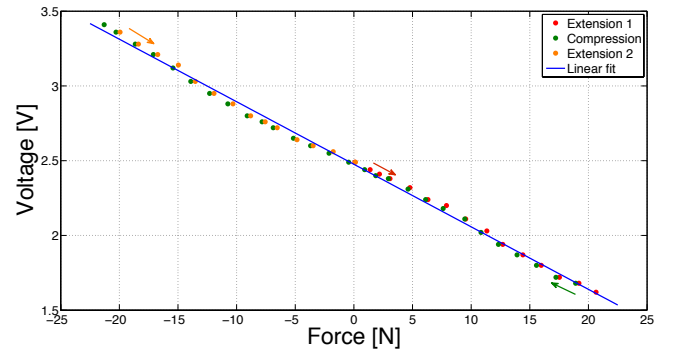

Fig. 10. Voltage measured by the Hall-effect sensor, as a function of interaction force. Arrows indicate the loading history.

employing the linear calibration derived in the previous section. Force control was implemented in blocked output conditions. The motor was voltage-controlled by a voltage amplifier (VoltPaq Q8, Quanser Inc.), using a causal PID controller[1], whose gains were tuned both theoretically (using a linear model of the controlled system) and experimentally in order to:

- avoid the presence of overshoot during step responses,
- guarantee a maximum of 1% steady state error,
- guarantee passivity of the developed controller [20].

A dynamic characterization experiment was conducted to determine the force regulation performances of the developed prototype. A Schroeder multisine signal with a peak value of 20 N (RMS value of 12 N) and constant spectral power density in the range [0.025, 10] Hz (negligible power content elsewhere) was specified as the desired force. The transfer function between desired and measured force for the controlled system was calculated using system identification methods in the frequency domain, and the estimated Bode plot is reported in Figure 11, that shows that the system has force control bandwidth of 7.4 Hz, and a phase delay lower than 35 deg in the controlled range.

IV. CONCLUSIONS AND FUTURE WORK

This paper has presented the design of a linear series elastic actuator, the basic element of the Series Elastic RiceWrist, a parallel manipulator with physical compliance that allows the implementation of force feedback interaction control strategies for wrist rehabilitation following stroke or incomplete spinal cord injury. The design specifications were presented and discussed, with an emphasis on the mechatronic design choices that allow the implementation of the desired force-feedback control strategies. The developed prototype achieved the desired performance in terms of accuracy of force measurement and capability of force

---

[1]Transfer function: $k_p + k_i \frac{1}{s} + k_d \frac{N}{1+\frac{N}{s}}$, $N = 100$
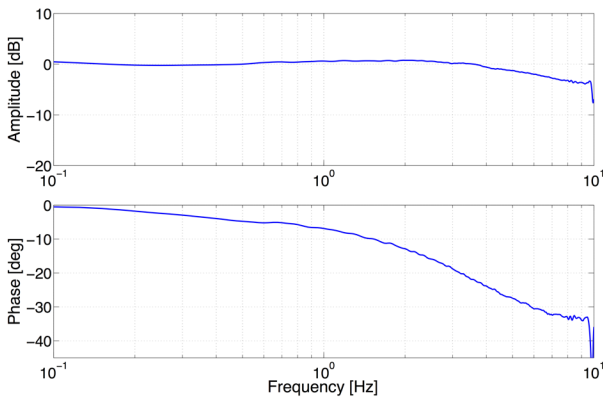

Fig. 11. Bode diagram of force control performances in blocked output conditions. Force control bandwidth is 7.4 Hz, with a correspondent phase lag of of 33 degrees. Transfer function estimation coherence drops below 0.9 for frequencies higher than 9 Hz.

feedback control over a range compatible with that of human movement assistance.

Future work will focus on the implementation of impedance control laws on the developed actuators and on the assembly of the 3DOF prototype, incorporating three of the developed linear SEAs in the actuation subsystem. Different strategies for impedance control in task space coordinates will be followed, namely considering either the SEAs as ideal force sources, or as ideal linear stiffness sources, that contribute to modulating different task-space coordinate stiffness.

REFERENCES

[1] N. Hogan and S. P. Buerger, "Interaction Control," *CRC Handbook on Robotics and Automation*, pp. 1–24, Aug. 2005.
[2] N. Hogan *et al.*, "Motions or muscles? Some behavioral factors underlying robotic assistance of motor recovery," *The Journal of Rehabilitation Research and Development*, vol. 43, no. 5, p. 605, 2006.
[3] R. van den Brand *et al.*, "Restoring Voluntary Control of Locomotion after Paralyzing Spinal Cord Injury," *Science*, vol. 336, no. 6085, pp. 1182–1185, May 2012.
[4] N. Hogan, "Impedance Control: An Approach to Manipulation," *Journal of Dynamic Systems, Measurement, and Control*, vol. 107, no. 1, pp. 1–24, Feb. 1985.
[5] B. Siciliano, L. Sciavicco, L. Villani, and G. Oriolo, *Robotics, Modelling, Planning and Control*. Springer, Feb. 2009.
[6] S. K. Charles and N. Hogan, "Dynamics of wrist rotations," *Journal of Biomechanics*, vol. 44, no. 4, pp. 614–621, 2011.
[7] D. Formica *et al.*, "The Passive Stiffness of the Wrist and Forearm," *Journal of neurophysiology*, vol. 108, no. 4, pp. 1158–1166, Aug. 2012.
[8] A. Deshpande, N. Gialias, and Y. Matsuoka, "Contributions of Intrinsic Visco-elastic Torques during Planar Index Finger and Wrist Movements," *Biomedical Engineering, IEEE Transactions on*, no. 99, pp. 1–1, 2012.
[9] M. M. Williamson, "Series Elastic Actuators," *PhD thesis, MIT*, pp. 1–83, Sep. 1995.
[10] D. W. Robinson, "Design and Analysis of Series Elasticity in Closed-loop," *PhD thesis, MIT*, pp. 1–123, Dec. 2000.
[11] A. Gupta, M. K. O'Malley, V. Patoglu, and C. Burgar, "Design, Control and Performance of RiceWrist: A Force Feedback Wrist Exoskeleton for Rehabilitation and Training," *The International Journal of Robotics Research*, vol. 27, no. 2, pp. 233–251, Feb. 2008.
[12] J. Rosen *et al.*, "The human arm kinematics and dynamics during daily activities-toward a 7 DOF upper limb powered exoskeleton," *Advanced Robotics, 2005. ICAR'05. Proceedings.*, pp. 532–539, 2005.
[13] H. I. Krebs *et al.*, "Robot-Aided Neurorehabilitation: A Robot for Wrist Rehabilitation," *IEEE Transactions on Neural Systems and Rehabilitation Engineering*, vol. 15, no. 3, pp. 327–335, Dec. 2007.
[14] F. Sergi *et al.*, "Design and characterization of a compact rotary Series Elastic Actuator for knee assistance during overground walking," *Biomedical Robotics and Biomechatronics (BioRob), 2012 4th IEEE RAS & EMBS International Conference on*, pp. 1931–1936, 2012.
[15] M. Mosadeghzad *et al.*, "Comparison of various active impedance control approaches, modeling, implementation, passivity, stability and trade-offs," in *Advanced Intelligent Mechatronics (AIM), 2012 IEEE/ASME International Conference on*, Jul. 2012, pp. 342–348.
[16] G. F. Wyeth, "Demonstrating the Safety and Performance of a Velocity Sourced Series Elastic Actuator," *2008 IEEE International Conference on Robotics and Automation*, pp. 3642–3647, May 2008.
[17] H. Vallery *et al.*, "Compliant actuation of rehabilitation robots," *Robotics & Automation Magazine, IEEE*, vol. 15, no. 3, pp. 60–69, Jan. 2008.
[18] C. Gosselin, "Stiffness mapping for parallel manipulators," *Robotics and Automation, IEEE Transactions on*, vol. 6, no. 3, 1990.
[19] J. P. Merlet, "Jacobian, Manipulability, Condition Number, and Accuracy of Parallel Robots," *Journal of Mechanical Design*, vol. 128, no. 1, p. 199, 2006.
[20] J. E. Colgate and N. Hogan, "Robust Control Of Dynamically Interacting Systems," *International Journal of Control*, vol. 48, no. 1, pp. 65–88, Jul. 1988.